Journal of Computational Electronics (2018) 17:1019–1028
https://doi.org/10.1007/s10825-018-1173-1

Design, modeling and analysis of dual-feed defected ground microstrip patch antenna with wide axial ratio bandwidth

Mukesh Kumar Khandelwal[1] · **Sachin Kumar**[2] · **Binod Kumar Kanaujia**[3]

Published online: 16 April 2018

Abstract
In this paper, a low profile microstrip patch antenna with defected ground structure is proposed for wide impedance and axial ratio bandwidth. The antenna structure consists of two feed lines with a circular defect loaded in the ground surface. The proposed antenna shows an impedance bandwidth of 71.92% ranging from 8.95 to 19 GHz covering X, Ku and K band applications. The mutual coupling between the two feed lines is suppressed by means of a single and double arc-shaped defect embedded in the ground plane. The mutual coupling is suppressed to a level of −37.5 dB with improved radiation performance. The measured 3-dB axial ratio bandwidth of the proposed antenna ranges from 8.85 to 11 GHz. An equivalent circuit model of the designed antenna is also proposed for theoretical analysis and theoretical results are verified with simulated and measured results.

Keywords Circular polarization (CP) · Defected ground structure (DGS) · Mutual coupling · Wideband

1 Introduction

Due to the rapid expansion of wireless communication, there is an increasing demand for antennas that provide high gain as well as polarization diversity along with wideband operation. To fulfill all these requirements, considerable attention has been given to circularly polarized (CP) antennas because they have the ability to suppress the detrimental effect of multipath fading and also they allow the signal reception caused by misalignment of receiving and transmitting antennas. CP planar antennas are most popularly used nowadays in portable handheld terminals because of their low profile, small size, cheap cost and easy integrability with handheld devices. There is no problem of orientation between transmitting and receiving elements involving CP antennas. CP antennas resolve the problem of fading leading to a system with better spectral efficiency and more throughput. A classical method for stimulating circular polarization involves excitation of two linearly polarized orthogonal modes of identical amplitude with quadrature phase difference between them.

A CP band can be excited by single feed or dual feed. A number of techniques have been presented by different researchers for the excitation of circular polarization by means of cutting a portion of the square radiator, inserting a slot, slit or stub in the ground or patch, by loading an active device in the patch, etc. [1–10]. A patch antenna with unobtrusive single feed and loaded metamaterial is proposed in Ref. [1]. This antenna consists of right/left-handed mushroom-shaped resonators for exciting circular polarization. In Ref. [2], circular polarization is achieved by loading parasitic shorting element. In Ref. [3], a single feed patch antenna loaded with U-slot and truncated corner square patch is proposed for circular polarization radiation. Single feed techniques provides a narrow axial ratio bandwidth. To achieve a broad bandwidth, a dual-fed L-shaped structure with cavity backing is reported in Ref. [4]. The ground plane with cavity backing helps in improving the coupling factor thus increasing the antenna bandwidth. CP

✉ Sachin Kumar
gupta.sachin0708@gmail.com

Mukesh Kumar Khandelwal
mukesh.khandelwal89@ieee.org

Binod Kumar Kanaujia
bkkanaujia@ieee.org

[1] Department of Electronics and Communication Engineering, Bhagwan Parshuram Institute of Technology, Rohini, Delhi 110089, India

[2] Department of Electronics and Communication Engineering, SRM Institute of Science and Technology, Chennai, Tamil Nadu 603203, India

[3] School of Computational and Integrative Sciences, Jawaharlal Nehru University, New Delhi 110067, India

can also be achieved by parasitic loading [5] or by inserting stubs [6]. Dual band CP operation is realized by introducing a parasitic patch under the radiating patch in Ref. [5] whereas in Ref. [6] L-shaped stubs are loaded exterior to the trimmed patch so that outer and inner mode can be excited. By introducing asymmetrical slits on each corner of square patch, circular polarization is achieved in Ref. [7,8]. For size reduction and to acquire circular polarization, arrowhead-shaped slotted antenna is proposed in Ref. [9]. The Koch fractal geometry can also be used for circular polarization [10]. The dual-feed configuration provides wider axial ratio bandwidth keeping quadrature phase difference between the two feed elements. However, the major problem lying with dual-feed antennas is mutual coupling between the two feed elements.

The problem of mutual coupling can be solved by using defected ground structure technique consequently improving the antenna performance parameters. In the last decade, a number of studies have been reported for reducing the mutual coupling effect using ground with induced defects. In Ref. [11], a circular ring is embedded in the ground surface for reducing the mutual coupling effect. In Ref. [12] the ground plane is loaded with a dumbbell shaped slot. A spiral-shaped ground with a defect is proposed in Ref. [13]. Finally, an inverted defective U-shaped ground in discussed in Ref. [14]. In this paper, we propose a dual-feed microstrip antenna with wide impedance and axial ratio bandwidth for X, Ku and K band satellite applications. The two microstrip line-feeds excites two orthogonal waves of same amplitude with a 90-degree phase difference between them for circular polarization. The mutual coupling effect between the feeds is minimized by integrating a pair of circular arc in the ground surface of the designed antenna. The proposed antenna shows a -10 dB impedance bandwidth of 71.92% ranging from 8.95 to 19 GHz and 3-dB axial ratio bandwidth from 8.85 to 11 GHz. The main advantage of proposed antenna is its low profile and simple geometry without any loading of active devices, truncation at corners or perturbations in the patch for exciting CP radiations. Moreover, the proposed antenna structure has been theoretically analyzed using the cavity model and equivalent circuit approach.

2 Antenna design

The antenna consists of a microstrip line of length L_{ml} and width w_{ml} with circular slot of radius a embedded in the ground plane underneath the open end of microstrip line as shown in Fig. 1. The antenna is referred as *Ant1* and the total size of antenna is $D \times D \times h$ mm^3. In the second step, one more microstrip line of same dimension (*Ant1*) is placed orthogonal to the first feed line and designed antenna is referred as *Ant2*. The dual-fed circular slot defected ground

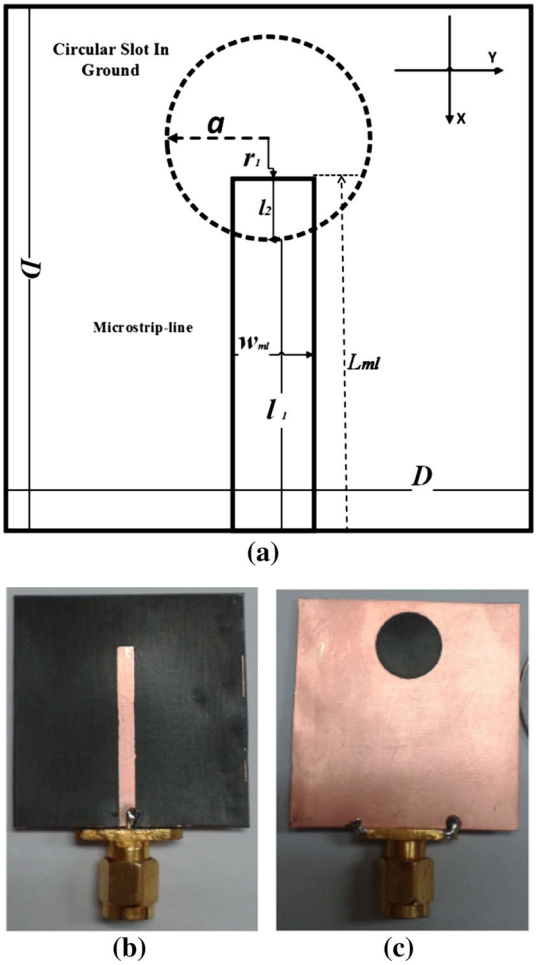

Fig. 1 Design layout of *Ant1* **a** schematic, **b** top view of fabricated prototype, **c** bottom view of fabricated prototype

antenna schematic and fabricated prototype is shown in Fig. 2. The two feeds are represented as *feed1* and *feed2*. The overall size of designed antenna is $B \times B \times h$ mm^3.

Further, in order to achieve circular polarization in the designed antenna (*Ant2*), the length of *feed2* is increased by a deference of quarter wavelength, thus introducing a phase shift of 90 degree between the resonating modes. The designed structure with asymmetric length dual-feed arrangement is referred as *Ant3*. Figure 3a, b shows the schematic and fabricated prototype of proposed *Ant3* with overall antenna size $B \times B_1 \times h$ mm^3 respectively. Additionally, to reduce the effect of mutual coupling between the feed lines, a circular arc-shaped slot of width s is embedded in the ground plane at a distance of d from the center of circular defect. The dual-fed circular arc-shaped slot loaded defected ground antenna schematic and fabricated prototype is shown in Fig. 3c, d, respectively, and is referred as *Ant4*. To further reduce the mutual coupling effect between the feed lines, one more slot (which is a mirror image of circular arc-shaped slot embedded in *Ant4*) is loaded in the designed antenna. The

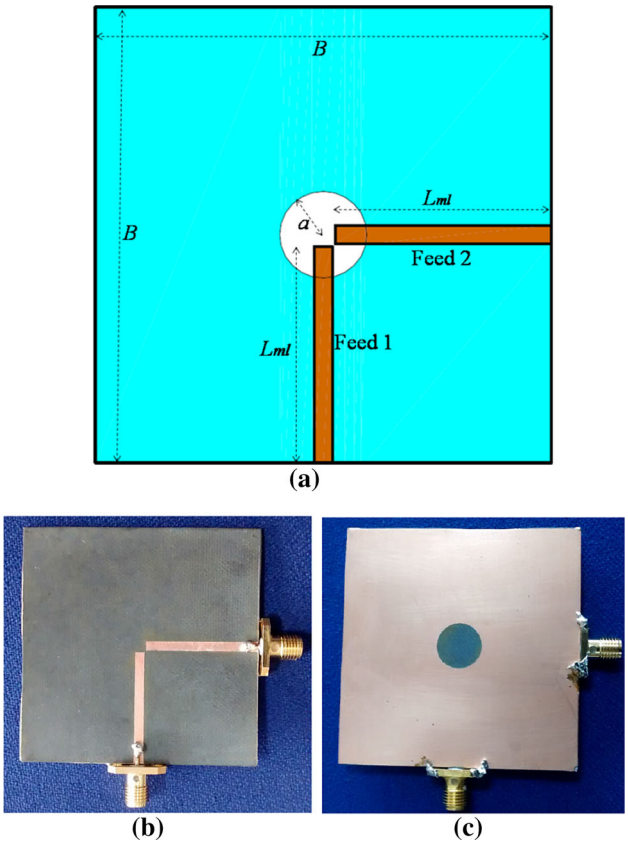

Fig. 2 Design layout of *Ant2* **a** schematic, **b** top view of fabricated prototype, **c** bottom view of fabricated prototype

dual-feed antenna loaded with two arc-shaped slots and circular defect in ground surface is referred as *Ant5*. Figure 3e, f shows the schematic and prototype of proposed *Ant5*, respectively. The simulation and optimization of proposed antenna prototype are carried out using finite element method based commercially available software package, Ansys HFSS. The detailed dimensions of the proposed structure are listed in Table 1.

3 Theoretical considerations

The equivalent circuit of microstrip line-fed defected ground antenna is illustrated in Fig. 4. Microstrip line of 50 Ω is used for feeding the antenna structure. The ground plane embedded circular defect radius a can be calculated as [15]

$$a = \frac{F}{\left\{1 + \frac{50h}{\pi\varepsilon_r F}\left[\ln\left(\frac{\pi F}{50h}\right) + 1.7726\right]\right\}^{1/2}} \tag{1}$$

where h and ε_r are the thickness and dielectric constant of the substrate, respectively. The value of F is calculated as

$$F = \frac{8.791 \times 10^9}{f_{\min}\sqrt{\varepsilon_r}} \tag{2}$$

where $f_{\min}$ is the design frequency of the wideband microstrip antenna. A deference of quarter wavelength is present in feed lines length for the excitation of circular polarization. The length L_{ml} of *feed1* and L_{ml2} of *feed2* are considered in the multiple of quarter wavelength and are calculated as

$$L_{\mathrm{ml}} = l_1 + l_2 = \frac{5}{4}\lambda_{\mathrm{eff}} \tag{3}$$

$$L_{\mathrm{ml2}} = \frac{5}{4}\lambda_{\mathrm{eff}} + \frac{1}{4}\lambda_{\mathrm{eff}} = \frac{3}{2}\lambda_{\mathrm{eff}} \tag{4}$$

where

$$\lambda_{\mathrm{eff}} = \frac{c}{f_{\min}\sqrt{\varepsilon_{\mathrm{eff}}}} \tag{5}$$

where c is the speed of light in free space and $\varepsilon_{\mathrm{eff}}$ is the effective dielectric constant of the microstrip line [15]

$$\varepsilon_{\mathrm{eff}} = \frac{\varepsilon_r + 1}{2} + \frac{\varepsilon_r - 1}{2}\frac{1}{\sqrt{1 + 12h/w_{\mathrm{ml}}}} \tag{6}$$

where w_{ml} is the width of microstrip line.

To calculate the position of circular defect embedded in the ground plane, the microstrip line has been divided into two parts: length l_1 and length l_2. A lossy microstrip line can be modeled as a tank circuit with parameters series resistance R, series inductance L, shunt conductance G and shunt capacitance C. These parameters R, L, G and C are in per unit length and can be calculated for length l_1 and l_2 for microstrip line. The parameters R_{11}, L_{11}, G_{11}, C_{11} and R_{12}, L_{12}, G_{12}, C_{12} correspond to the microstrip line of length l_1 and l_2 of *feed1*, respectively. Similarly, the parameters R_{21}, L_{21}, G_{21}, C_{21} and R_{22}, L_{22}, G_{22}, C_{22} correspond to microstrip line of length l_1 and l_2 of *feed2*, respectively. The microstrip line impedance Z_{11} and Z_{12} of *feed1* and Z_{21} and Z_{22} of *feed2* offered by length l_1 and l_2, respectively, are given as

$$Z_{11} = \sqrt{\frac{R_{11} + j\omega L_{11}}{G_{11} + j\omega C_{11}}} \tag{7}$$

$$Z_{12} = \sqrt{\frac{R_{12} + j\omega L_{12}}{G_{12} + j\omega C_{12}}} \tag{8}$$

$$Z_{21} = \sqrt{\frac{R_{21} + j\omega L_{21}}{G_{21} + j\omega C_{21}}} \tag{9}$$

$$Z_{22} = \sqrt{\frac{R_{22} + j\omega L_{22}}{G_{22} + j\omega C_{22}}} \tag{10}$$

A fringing capacitance C_{f} gets introduced at the open-ended discontinuity of the microstrip line which is calculated as [16]

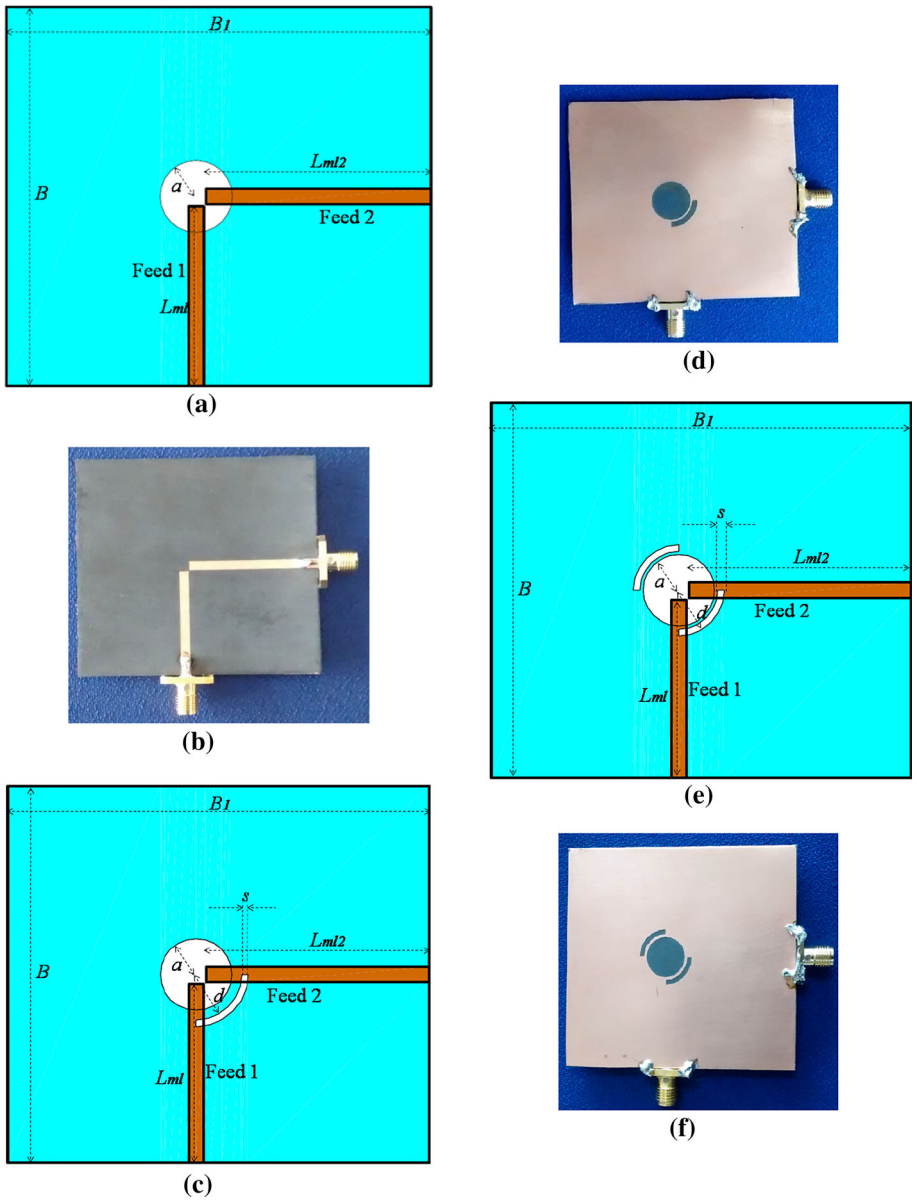

Fig. 3 Design layout of the proposed antennas **a** schematic of *Ant3*, **b** fabricated prototype of *Ant3* (top view), **c** schematic of *Ant4*, **d** fabricated prototype of *Ant4* (bottom view), **e** schematic of *Ant5*, **f** fabricated prototype of *Ant5* (bottom view)

Table 1 Design specifications for proposed antennas

Parameter	mm	Parameter	mm	Parameter	mm
a	5.5	w_{ml}	2.3	s	1
r_1	1.5	D	36	d	6
l_1	23.41	B	57.83	h	0.762
l_2	4	B_1	64.68		
L_{ml}	27.41	L_{ml2}	34.27		

$$C_f = \frac{\Delta l \sqrt{\varepsilon_{\mathrm{eff}}}}{c Z_0} \tag{11}$$

where Δl is the extended fringing field length at the end of microstrip line and Z_0 is the characteristic impedance of microstrip line. The impedance offered by fringing capacitance of *feed1* and *feed2* referred as Z_{f1} and Z_{f2} respectively which is determined as

$$Z_{\mathrm{f1}} = Z_{\mathrm{f2}} = \frac{1}{j\omega C_{\mathrm{f}}} \tag{12}$$

The coupling between the two circuits can be modeled by the help of coupling capacitance C_{p} given by [17]

$$C_{\mathrm{p}} = \frac{-(C_1 + C_2) + \sqrt{(C_1 + C_2)^2 - 4C_1C_2\left(1 - C_k^{-2}\right)}}{2} \tag{13}$$

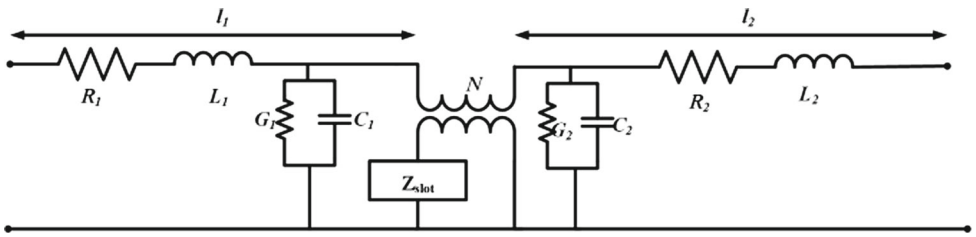

Fig. 4 Modeling of DGS with microstrip line

where C_1 and C_2 are the capacitances offered by both the circuits. The coupling coefficient C_k between the two networks is

$$C_k = \frac{1}{\sqrt{Q_1 Q_2}} \tag{14}$$

where Q_1 and Q_2 are the quality factor in both the networks. The coupling capacitance between *feed1* and circular defect is referred as C_{p1}. Similarly, the coupling capacitance between *feed2* and circular defect is referred as C_{p2}. To model the coupling between fringing fields due to two feed lines, a coupling capacitance C_{ff} is introduced in the circuit model. A coupling capacitance C_{PC} between both the feed lines is also introduced. The coupling capacitance values may be calculated by the help of Eq. (13). The quality factor of microstrip line is determined as

$$Q = \omega \frac{L}{R} \tag{15}$$

The coupling capacitance C_{p1}, C_{p2}, C_{ff} and C_{PC} offers Z_{p1}, Z_{p2}, Z_f and Z_{PC} impedance, respectively, which can be calculated as

$$Z_{P1} = \frac{1}{j\omega C_{p1}};\ Z_{P2} = \frac{1}{j\omega C_{p2}};\ Z_f = \frac{1}{j\omega C_{ff}};$$
$$Z_{PC} = \frac{1}{j\omega C_{PC}} \tag{16}$$

The coupling inductance L_{PL} between the two microstrip lines is determined from [17]

$$L_{PL} = \frac{C_k{}^2 (L_1+L_2) + \sqrt{C_k{}^2 (L_1+L_2)^2 + 4C_k{}^2 \left(1-C_k{}^2\right) L_1 L_2}}{2\left(1-C_k{}^2\right)} \tag{17}$$

where L_1 and L_2 represents the inductance of *feed1* and *feed2*, respectively. The impedance offered by coupling inductance L_{PL} is calculated as

$$Z_{PL} = j\omega L_{PL} \tag{18}$$

The input impedance Z_{slot} of embedded ground slot is modeled by an ideal transformer with microstrip line as shown in Fig. 4. The turn ratio N of transformer is determined as [18]

$$N = \sqrt{\frac{Z_0}{Z_{slot}}} \tag{19}$$

The slot impedance Z_{slot} of circular defect is calculated from [19]

$$Z_{slot} = \frac{\eta^2}{4Z_{cy}} \tag{20}$$

where η is the intrinsic impedance, Z_{cy} is input impedance of the cylindrical dipole given as

$$Z_{cy} = R_r\,(kl) - j\left[120\left(ln\frac{l}{w} - 1\right)\cot\frac{kl}{2}\right] \tag{21}$$

where R_r is defined as the radiation resistance of the dipole determined as

$$R_r = \frac{\eta_0}{2\pi}\int_0^{\pi}\left[\frac{\left[\cos\left(\frac{k^2}{2}\cos\theta\right) - \cos\left(\frac{kl}{2}\right)\right]^2}{\sin\theta}\right] d\theta \tag{22}$$

The slot is integrated in the ground plane; thus, the input impedance of the slot is added to the circuit model by an ideal transformer with turn ratio N determined by

$$Z\prime_{slot} = N Z_{slot} \tag{23}$$

Figure 5 shows the equivalent circuit model for the proposed antenna structure. The total input impedance Z_{in} of the model is given by

$$Z_{in} = \left[\left(\frac{1}{(Z_{11}+Z_{12})} + \frac{1}{Z_{P1}} + + \frac{1}{Z_{f1}} + \frac{1}{Z'_{slot}}\right) + \left(\frac{1}{Z_{PL}} + \frac{1}{Z_f} + \frac{1}{Z_{PC}}\right) + \left(\frac{1}{(Z_{21}+Z_{22})} + \frac{1}{Z_{P2}} + \frac{1}{Z_{f2}}\right)\right]^{-1} \tag{24}$$

The S_{11} value of proposed antenna is calculated as

$$S_{11} = 20\log(|r|) \tag{25}$$

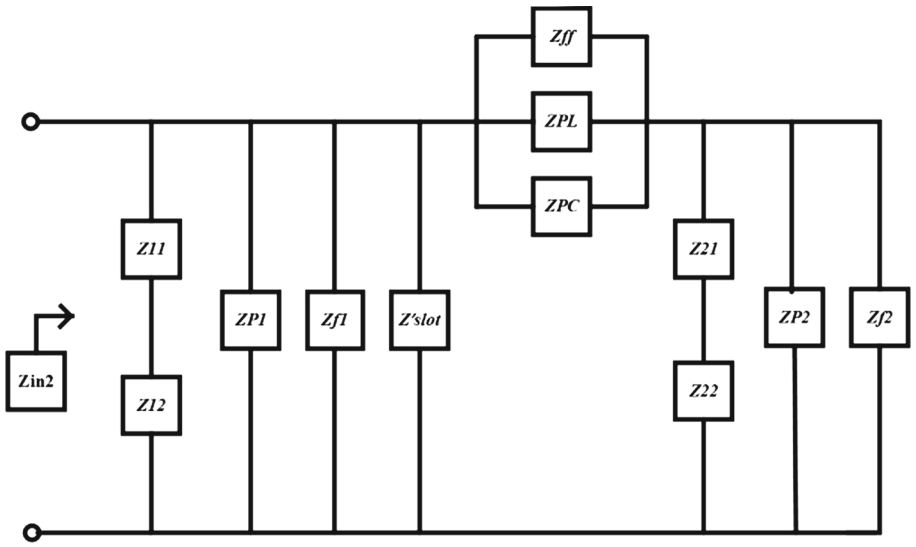

Fig. 5 Equivalent circuit model for the proposed antenna structure

where r is the reflection coefficient and is

$$\mathrm{r} = \frac{Z_{\mathrm{in}} - Z_0}{Z_{\mathrm{in}} + Z_0} \tag{26}$$

The voltage standing wave ratio (VSWR) can be calculated as

$$\mathrm{VSWR} = \frac{1 + |\mathrm{r}|}{1 - |\mathrm{r}|} \tag{27}$$

The parameters for each port can be calculated using Eqs. (24–27) i.e. Z_{in1}, S_{11}, r_1, VSWR_1 and Z_{in2}, S_{22}, r_2, VSWR_2 corresponding to port 1 and port 2, respectively. The parameter S_{12} or S_{21} is related with other parameters by following equation [20]

$$Z_{\mathrm{in1}} = Z_0 \frac{(1+S_{11})(1-S_{22}) + S_{21}^2 + 2S_{21}\frac{\mathrm{VSWR}_2(1-S_{22}) - \mathrm{VSWR}_1 S_{21}}{\mathrm{VSWR}_1(1-S_{11}) - \mathrm{VSWR}_2 S_{21}}}{(1-S_{11})(1-S_{22}) - S_{21}^2} \tag{28}$$

The parameter S_{21} can be easily calculated by Eq. (28) after calculating Z_{in}, S_{11}/S_{22} and VSWR using Eqs. (24), (25) and (27), respectively.

4 Results and discussion

The substrate RT Duriod 5880 is used for the fabrication of all proposed antenna designs. The dielectric constant ε_{r}, loss tangent $tan\ \delta$ and height h of the substrate are 2.2, 0.0009 and 0.762 mm, respectively. The S-parameters of the fabricated antennas are measured using Agilent Vector Network Analyzer PNA L series. The theoretical, simulated and measured return loss behavior of *Ant1* is shown in Fig. 6 and is considered as a reference antenna for the present study.

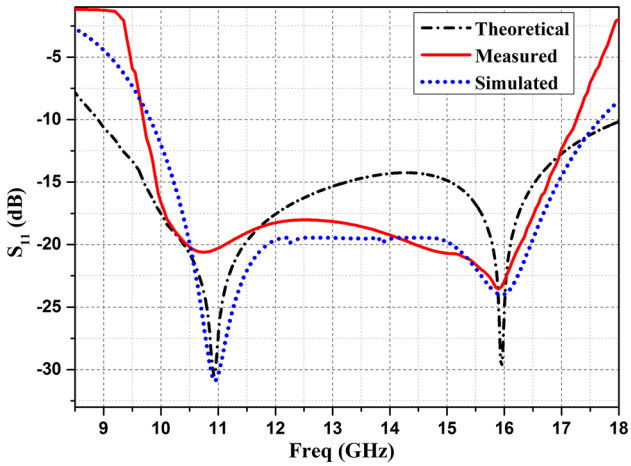

Fig. 6 Theoretical, simulated and measured S-parameters of *Ant1*

Ant1 shows two resonances at 10.8 and 16 GHz with wide impedance bandwidth ranging from 9.8 to 17.55 GHz.

The *Ant2* with microstrip line dual-feed mechanism shows an impedance bandwidth ranging from 9.1 to 14.95 GHz with single resonance at 10.15 GHz. The S-parameter variation of *Ant2* is shown in Fig. 7, and an impedance bandwidth of 48.65% is achieved in this antenna. The mutual coupling between the two feed lines degrades the antenna performance resulting in a smaller − 10 dB impedance bandwidth and single resonance in *Ant2* compared to *Ant1*. Because of a small distance between the open ends of two microstrip lines, a large amount of mutual coupling will be present among the feed lines. The S_{21} of *Ant2* is about − 12.87 dB at 12 GHz. The theoretical, simulated and measured S-parameters of *Ant2* are in good agreement with each other. However, compared to simulated and measured results, the theoretical S_{11} variation shows better resonance at 11.4 GHz. This can be understood by the concept of current distribution within

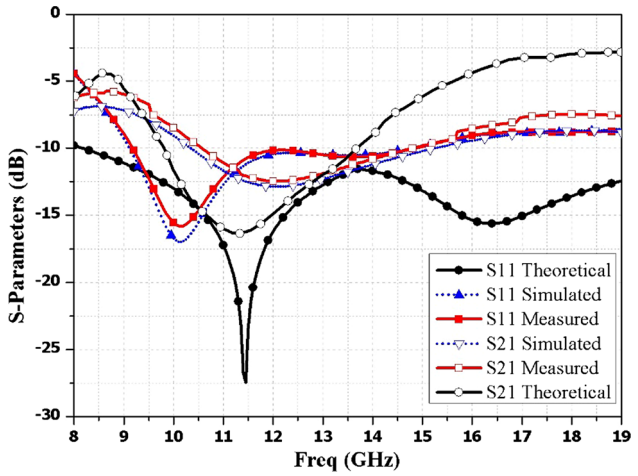

Fig. 7 Theoretical, simulated and measured S-parameters of *Ant2*

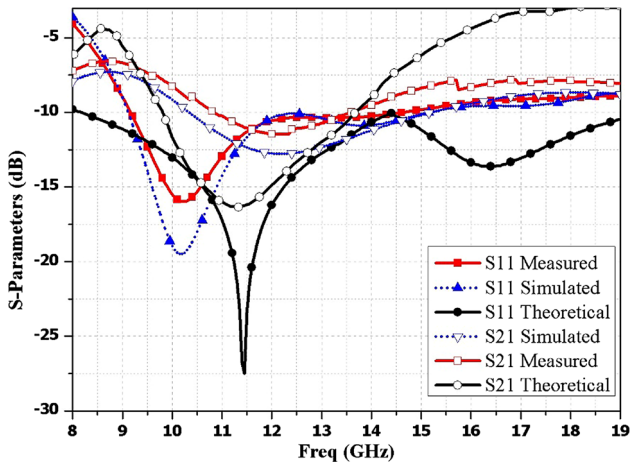

Fig. 8 Theoretical, simulated and measured S-parameters of *Ant3*

the metal strip and the ground plane. The presence of ground plane under the feed line results in an unequal division of current in the metal conductor and the ground surface. Because of this the normalized series resistance offered by the strip and the ground are of different values. Since there is no ground plane under the length l_2, the normalized series resistance offered by this segment is negligible.

The theoretical, simulated and measured S-parameters of *Ant3* are shown in Fig. 8. There is a difference of $\lambda/4$ between the two rectangular feed lines in *Ant3*. *Ant3* shows an impedance bandwidth of 52.53% ranging from 9.1 to 15.25 GHz. The mutual coupling S_{21} between the two feed lines is almost same as in *Ant2*. In Fig. 8, the measured and simulated S_{11} variations are in good match with theoretical results.

Figure 9 shows simulated and measured return loss comparison for *Ant4*. The -10 dB impedance bandwidth ranges from 8.95 to 19 GHz (71.92%). The parametric comparisons of S_{11} with frequency for different values of circular arc width s and radius d are shown in Figs. 10 and 11, respectively. The

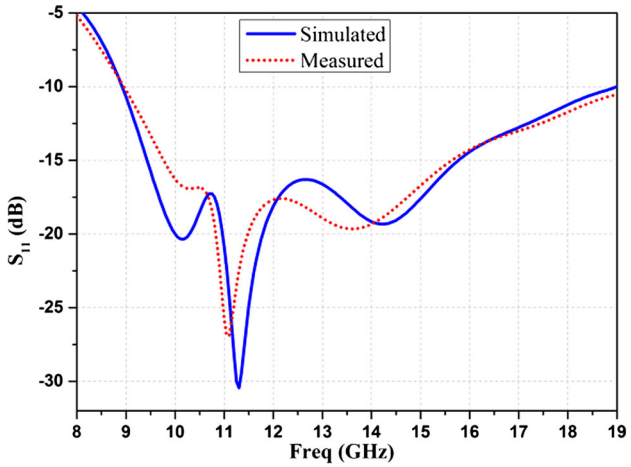

Fig. 9 Simulated and measured S_{11} variation with frequency of *Ant4* ($d = 6$ mm and $s = 1$ mm))

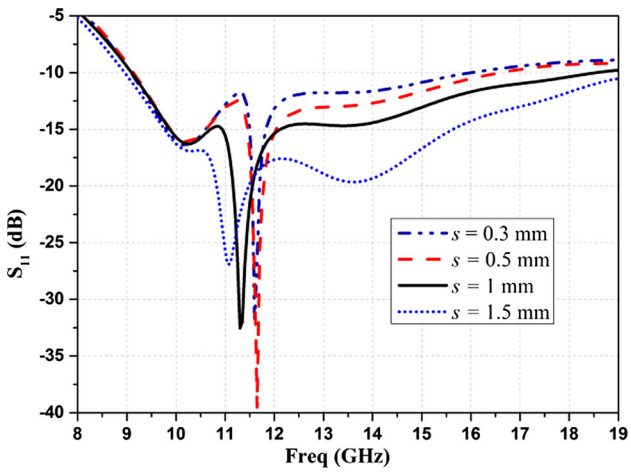

Fig. 10 S_{11} variation with frequency of *Ant4* for different arc width

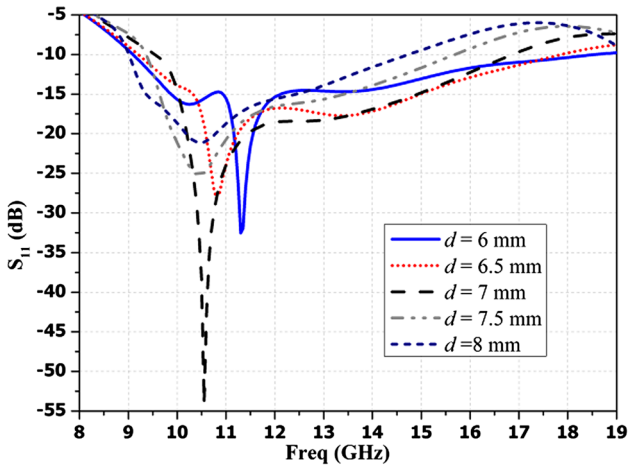

Fig. 11 S_{11} variation with frequency of *Ant4* for different arc position

mutual coupling comparisons for different values of circular arc width s and radius d are shown in Figs. 12 and 13,

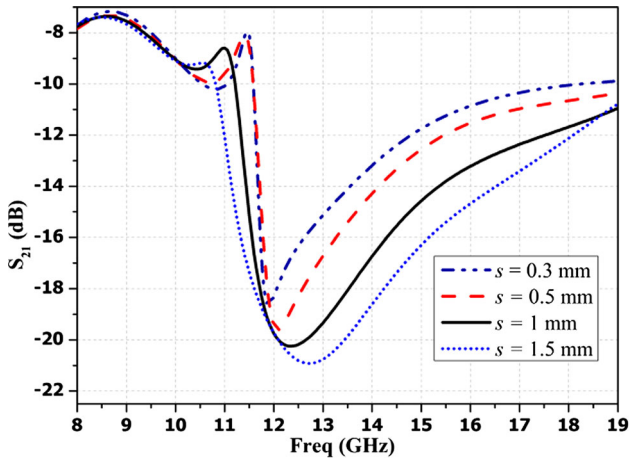

Fig. 12 S_{21} variation with frequency of *Ant4* for different arc width

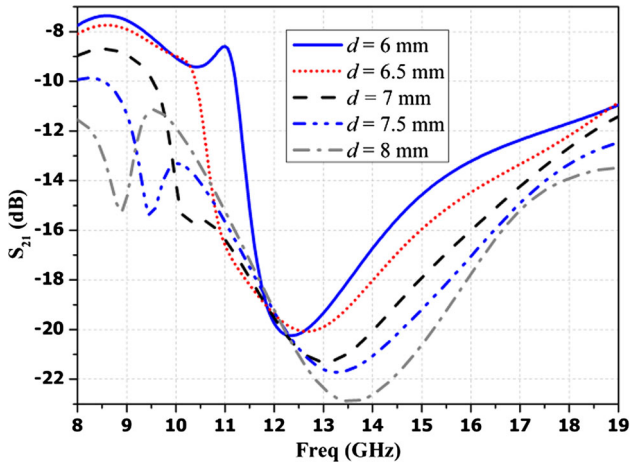

Fig. 13 S_{21} variation with frequency of *Ant4* for different arc position

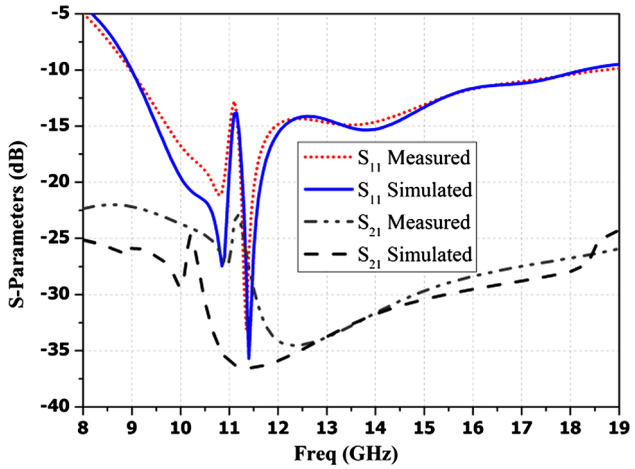

Fig. 14 Simulated and measured S-parameters of *Ant5*

respectively. In the figure, it can be observed that the value of S_{21} is suppressed to a level of -20.3 dB for $s = 1$ mm and $d = 6$ mm.

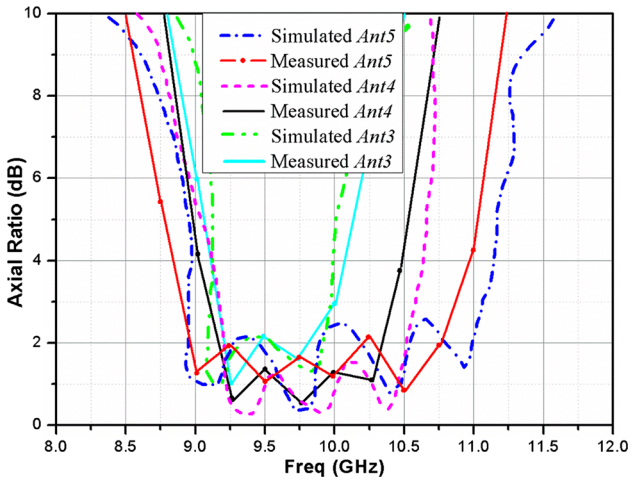

Fig. 15 Simulated and measured axial ratio of *Ant3*, *Ant4*, *Ant5*

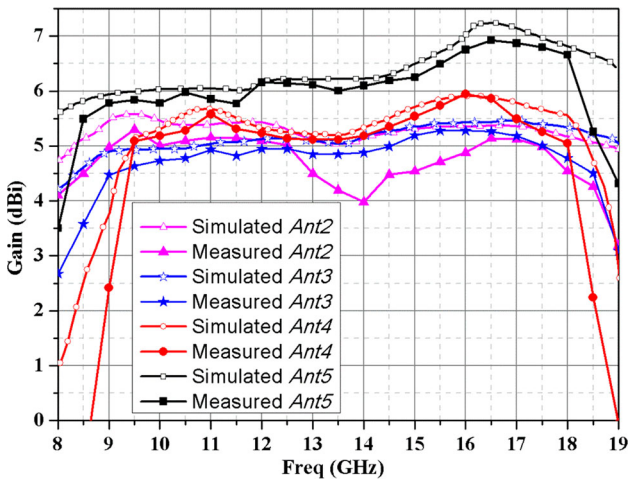

Fig. 16 Simulated and measured gain of *Ant2*, *Ant3*, *Ant4*, *Ant5*

The S-parameters variation with frequency for *Ant5* is shown in Fig. 14. *Ant5* shows an impedance bandwidth of 71.92% ranging from 8.95 to 19 GHz. By embedding two circular arcs in the ground plane, the mutual coupling value can be suppressed up to a level of -37.5 dB in the band of operation. The simulated results of proposed antenna are in good match with measured results. The S_{22} and S_{12} variations of all the designed antennas are similar to their relative S_{11} and S_{21} variations; therefore, in order to avoid the repetition of figures, S_{11} and S_{21} parameters have been shown only.

Figure 15 illustrates the axial ratio variation with frequency of *Ant3*, *Ant4* and *Ant5*. For creating a 90-degree phase difference between the resonating modes, a pair of feed lines with a difference of quarter wavelength between the two are used. *Ant3* shows circular polarization ranging from 9.1 to 10 GHz. The 3-dB axial ratio value of *Ant4* ranges from 9.15 to 10.35 GHz with a wide band of more than 1.2 GHz.

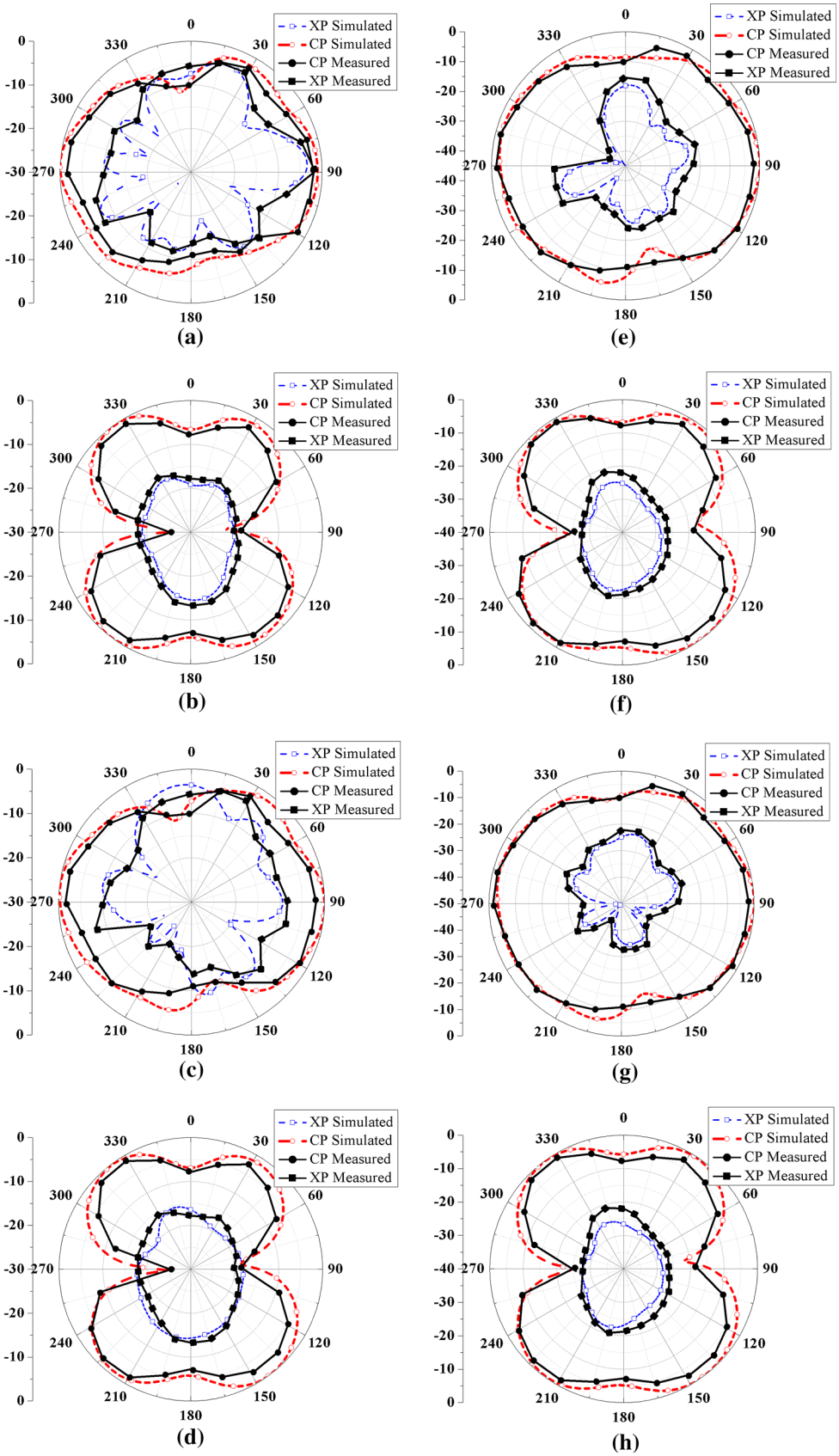

Fig. 17 Simulated and measured Co-Polar (CP) and Cross-Polar (XP) radiation pattern at 10 GHz **a** *Ant2* in XY plane, **b** *Ant2* in XZ plane, **c** *Ant3* in XY plane, **d** *Ant3* in XZ plane, **e** *Ant4* in XY plane, **f** *Ant4* in XZ plane, **g** *Ant5* in XY plane, **h** *Ant5* in XZ plane

The measured 3-dB axial ratio bandwidth of *Ant5* ranges from 8.85 to 11 GHz with a wide bandwidth of more than 2.1 GHz. Thus, *Ant5* provides largest 3-dB axial ratio bandwidth among the proposed dual-feed antenna designs.

The gain of proposed antennas *Ant2*, *Ant3*, *Ant4* and *Ant5* is shown in Fig. 16. *Ant2* and *Ant3* show peak gain of 5.2 and 5.4 dBi at resonance frequencies 9.5 and 16.6 GHz, respectively. The average gain of *Ant2* and *Ant3* is about 5.2 and 5 dBi, respectively, within the radiating band. An increase in the value of gain is observed in *Ant4* at the frequency 16 GHz due to the isolation effect provided by the embedded circular arc. A further improvement in antenna gain is observed in *Ant5* by means of a double arc-shaped embedded defect in the ground surface. The peak values of measured gain in *Ant4* and *Ant5* are 5.9 and 6.9 dBi, respectively. A small difference in simulated and measured results is present due to conventional photolithography fabrication process, soldering of SMA connectors and cable effects. Figure 17 shows the Co-Polar (CP) and Cross-Polar (XP) radiation characteristics of presented antennas in XY and XZ planes. For comparison purpose, all radiation patterns are plotted at 10 GHz. *Ant2* and *Ant3* show higher XP level because of dual feed, whereas XP level is suppressed in *Ant4* and *Ant5* because of the use of DGS. *Ant5* shows best radiation characteristics with minimum XP level and better isolation between CP and XP radiations.

5 Conclusion

A dual-feed microstrip patch antenna with wide -10 dB impedance and 3-dB axial ratio bandwidth is presented. The dual feeds stimulate the two orthogonal waves with 90-degree phase difference among them to obtain circular polarization without cutting or notching any region of the radiating patch. An equivalent circuit model is also proposed for the antenna structure, and it is found that theoretical and simulated results are a good match with measured results. Further, single and double arc-shaped DGS are embedded in the ground plane to reduce the mutual coupling effect between the feed lines. The antenna shows a wide impedance bandwidth of 71.92% ranging from 8.95 to 19 GHz with a measured peak gain of around 6.9 dBi in the resonating band. The proposed antenna does not involve truncation of corners or any loading of active devices used for the excitation of circular polarization. Compared with the other existing wideband CP antennas, the presented antenna is very easy to fabricate as well as has wide impedance and axial ratio bandwidth, thus making it a potential candidate for the current wireless applications.

References

1. Dong, Y., Toyao, H., Itoh, T.: Compact circularly-polarized patch antenna loaded with metamaterial structures. IEEE Trans. Antennas Propag. **59**(11), 4329–4333 (2011)
2. Wong, H., So, K.K., Ng, K.B., Luk, K.M., Chan, C.H., Xue, Q.: Virtually shorted patch antenna for circular polarization. IEEE Antennas Wirel. Propag. Lett. **9**, 1213–1216 (2010)
3. Lam, K.Y., Luk, K.M., Lee, K.F., Wong, H., Ng, K.B.: Small circularly polarized U-Slot wideband patch antenna. IEEE Antennas Wirel. Propag. Lett. **10**, 87–90 (2011)
4. Liu, Y., Chen, S., Ren, Y., Cheng, J., Liu, Q.H.: A broadband proximity-coupled dual-polarized microstrip antenna with L-shape backed cavity for X-band applications. AEU-Int. J. Electron. Commun. **69**(9), 1226–1232 (2015)
5. Deng, C., Li, Y., Zhang, Z., Pan, G., Feng, Z.: Dual-band circularly polarized rotated patch antenna with a parasitic circular patch loading. IEEE Antennas Wirel. Propag. Lett. **12**, 492–495 (2013)
6. Chen, C.H., Yung, E.K.N.: A novel unidirectional dual-band circularly-polarized patch antenna. IEEE Trans. Antennas Propag. **59**(8), 3052–3057 (2011)
7. Gautam, A.K., Kanaujia, B.K.: A novel dual-band asymmetric slit with defected ground structure microstrip antenna for circular polarization operation. Microw. Opt. Technol. Lett. **55**(6), 1198–1201 (2013)
8. Gautam, A.K., Benjwal, P., Kanaujia, B.K.: A compact square microstrip antenna for circular polarization. Microw. Opt. Technol. Lett. **54**(4), 897–900 (2012)
9. Gautam, A.K., Kunwar, A., Kanaujia, B.K.: Circularly polarized arrowhead-shape slotted microstrip antenna. IEEE Antennas Wirel. Propag. Lett. **13**, 471–474 (2014)
10. Farswan, A., Gautam, A.K., Kanaujia, B.K., Rambabu, K.: Design of Koch fractal circularly polarized antenna for handheld UHF RFID reader applications. IEEE Trans. Antennas Propag. **64**(2), 771–775 (2016)
11. Guha, D., Biswas, S., Joseph, T., Sebastian, M.T.: Defected ground structure to reduce mutual coupling between cylindrical dielectric resonator antennas. Electron. Lett. **44**(14), 836–837 (2008)
12. Zhu, F.G., Xu, J.D., Xu, Q.: Reduction of mutual coupling between closely-packed antenna elements using defected ground structure. Electron. Lett. **45**(12), 601–602 (2009)
13. Chung, Y., Jeon, S.-S., Ahn, D., Choi, J.-I., Itoh, T.: High isolation dual-polarized patch antenna using integrated defected ground structure. IEEE Microw. Wirel. Compon. Lett. **14**(1), 4–6 (2004)
14. Xiao, S., Tang, M.C., Bai, Y.Y., Gao, S., Wang, B.Z.: Mutual coupling suppression in microstrip array using defected ground structure. IET Microw. Antennas Propag. **5**(12), 1488–1494 (2011)
15. Garg, R., Bhartia, P., Bahl, I., Ittipiboon, A.: Microstrip Antenna Design Handbook. Artech House, Norwood (2001)
16. Tang, W., Chow, Y.L., Tsang, K.F.: Different microstrip line discontinuities on a single field-based equivalent circuit model. IEE Proc. Microw. Antennas Propag. **151**(3), 256–262 (2004)
17. Terman, F.E.: Electronic and Radio Engineering. McGraw Hill, New York (1955)
18. Caloz, C., Okabe, H., Iwai, T., Itoh, T.: A simple and accurate model for microstrip structures with slotted ground plane. IEEE Microw. Wirel. Compon. Lett. **14**(4), 133–135 (2004)
19. Wolff, E.A.: Antenna Analysis. Artech House, Norwood (1988)
20. Larsen, N.V., Breinbjerg, O.: An L-band, circularly polarised, dual-feed, cavity backed annular slot antenna for phased-array applications. Microw. Opt. Technol. Lett. **48**(5), 873–878 (2006)